Sustainable Energy & Fuels

ROYAL SOCIETY OF CHEMISTRY

PAPER

View Article Online
View Journal | View Issue

Check for updates

Cite this: *Sustainable Energy Fuels*, 2025, **9**, 4731

Enhancement of photothermal catalytic activity by suppression of thermal conduction in dry reforming of methane over silica-supported Ni catalysts†

Daichi Takami, [a] Hisao Yoshida [a] and Akira Yamamoto *[b]

As global energy demand continues to rise, the development of sustainable alternatives to fossil fuels has become increasingly critical. This study investigates the photothermal dry reforming of methane (PT-DRM) over Ni/SiO_2 catalysts mixed with various ceramics, focusing on the interplay between thermal conductivity and catalytic activity. Catalysts mixed with low thermal conductivity ceramics effectively suppressed heat dissipation from the light-irradiated surface, resulting in enhanced photothermal catalytic performance. Furthermore, the catalysts mixed with low light-absorbing ceramics, such as SiO_2, Al_2O_3 and AlN, exhibited reasonable catalytic activity relative to the measured surface temperature. In contrast, high light-absorbing ceramics such as SiC and TiC hindered efficient light absorption by the Ni nanoparticles (Ni NPs), resulting in lower catalytic activity than expected from the surface temperature. These results highlight the critical roles of thermal conductivity of catalysts and direct light absorption by active sites in optimizing photothermal catalysts, providing valuable insights for the design of advanced solar-driven catalytic systems for effective solar energy utilization and greenhouse gas mitigation.

Received 26th April 2025
Accepted 20th June 2025

DOI: 10.1039/d5se00594a

rsc.li/sustainable-energy

Open Access Article. Published on 20 June 2025. Downloaded on 25/11/2025 6:45:27 AM.
This article is licensed under a Creative Commons Attribution-NonCommercial 3.0 Unported Licence.

Introduction

In the face of a rapidly increasing global energy demand, society's heavy dependence on fossil fuels—such as coal, oil, and natural gas—raises significant sustainability challenges, given the finite availability and environmental impact of these resources.[1] To achieve sustainable development, it is essential to seek alternative renewable resources.[2] Solar energy with its virtually limitless supply is emerging as a promising candidate in this transition.[3] Consequently, numerous researchers have investigated methods for converting solar energy into electrical,[4–8] thermal,[9–12] or chemical[13–16] energies.

As an approach to converting light energy to chemical energy, photocatalytic methods have garnered considerable attention.[17–20] These processes rely on the absorption of photons to promote electronic transition, which activates specific catalytic sites. However, these approaches are often limited by the requirement for high-energy ultraviolet (UV) light, which constitutes only a tiny fraction of the solar spectrum.[21] Recently, the light-driven thermal (photothermal) approach to catalytic reactions has attracted attention due to its broader effective wavelength range, including visible and near-infrared (NIR) light, and versatility in various applications.[22–24]

One of the notable fields applying photothermal approaches is the dry reforming of methane (DRM, eqn (1)) reaction, an endothermic reaction that converts two potent greenhouse gases, carbon dioxide (CO_2) and methane (CH_4), into syngas, a mixture of carbon monoxide (CO) and hydrogen (H_2). Syngas is a versatile industrial feedstock for applications such as methanol synthesis and Fischer–Tropsch processes.[25]

$$CO_2 + CH_4 \rightarrow 2CO + 2H_2 \quad \Delta H^{\circ}_{298K} = 247\ \text{kJ mol}^{-1} \qquad (1)$$

In contrast to conventional DRM reaction, which requires significant thermal input to drive the reaction, the photothermal DRM (PT-DRM) reaction utilizes light energy to reduce external energy consumption. Enormous efforts have been devoted to exploring photothermal catalysts for the PT-DRM reaction. Especially, nickel (Ni) nanoparticles (NPs) catalysts have been extensively investigated due to their high catalytic activity, favourable optical properties, and relatively low cost.[26–46] However, challenges, such as severe coke deposition and sintering of Ni NPs, remain obstacles to practical application.[47]

[a]*Graduate School of Human and Environmental Studies, Kyoto University, Yoshida-Nihonmatsu-cho, Sakyo-ku, Kyoto 606-8501, Japan*

[b]*Department of Applied Chemistry, Faculty of Science and Engineering, Kindai University, 3-4-1, Kowakae, Higashiosaka, Osaka 577-8502, Japan. E-mail: yama@apch.kindai.ac.jp*

† Electronic supplementary information (ESI) available: The amounts of catalysts for photothermal activity tests, HR-TEM image, crystallite size of Ni metal, effect of the sample amount, temperature dependence of activity in the dark and comparison between estimated and measured temperature. See DOI: https://doi.org/10.1039/d5se00594a

Open Access Article. Published on 20 June 2025. Downloaded on 25/11/2025 6:45:27 AM. This article is licensed under a Creative Commons Attribution-NonCommercial 3.0 Unported Licence.

Further advancement of photothermal catalysts requires a more comprehensive understanding of photothermal conversion process and strategies to enhance efficiency. Recently, in our study on Ni/SiO_2 catalysts exhibiting high activity and stability for the PT-DRM reaction, we reported that increasing the Ni loading had two opposing effects on photothermal conversion efficiency of the catalysts: enhanced light absorption by Ni metal and accelerated heat dissipation due to its high thermal diffusivity.[37] This finding underscores the need to suppress thermal dissipation such as thermal conduction to maximize surface temperature for effective photothermal conversion. However, the increase in Ni loading also influences catalytic properties such as particle size, chemical state, and metal–support interactions, complicating the overall effect of thermal conductivity on catalytic activity.

Also, a central hypothesis in this field is that direct heat generation at the active sites (*e.g.* photothermal effect of Ni NPs) would be more efficient than indirect heating methods, such as the use of external photothermal materials. This direct heating approach could allow for efficient energy use by concentrating heat exactly where it is needed. However, this hypothesis remains untested, emphasizing the need for further research to validate and improve catalyst designs that enable effective localized heating in PT-DRM applications. In this study, we systematically examine the role of thermal conductivity and the effect of direct photothermal heating in the PT-DRM reaction by employing Ni/SiO_2 catalysts mixed with ceramics of various thermal conductivity to maintain the intrinsic catalytic properties of the Ni/SiO_2 catalyst.

Experimental

Catalyst preparation

The Ni/SiO_2 catalyst with 25 wt% Ni loading was prepared by the ammonia evaporation method using nickel carbonate basic (FUJIFILM Wako Pure Chemical Co, Tokyo, Japan), spherical SiO_2 (Sciqas 0.05 μm, Sakai Chemical Industry, Osaka, Japan), and 28% aqueous NH_3 solution (Nacalai Tesque, Kyoto, Japan). The suspension of these compounds was stirred at room temperature and heated to dryness at 353 K with stirring. The obtained powder was calcined at 723 K for 2 h. After that, the Ni/SiO_2 catalyst was physically mixed with SiO_2 (Sciqas 0.05 μm), α-Al_2O_3 (NP-ALO-1-100, EMJAPAN CO. LTD, Tokyo, Japan), AlN (aluminium nitride 50 nm, Wako Pure Chemical Co, Tokyo, Japan), SiC (silicon carbide β form 50 nm, FUJIFILM Wako Pure Chemical Co, Tokyo, Japan), or TiC (NP-TIC-2-100, EMJAPAN CO. LTD., Tokyo, Japan) in a 1 : 1 weight ratio for 15 minutes to prepare mixed catalysts. These ceramic powders are similar in size (~50 nm) to the spherical silica used for the preparation of Ni/SiO_2 catalysts. These mixed catalysts were denoted as Ni/SiO_2 + X (X: SiO_2, Al_2O_3, AlN, SiC or TiC)

Characterisation

UV/visible/NIR diffuse reflectance (DR) spectroscopy was conducted with a V-570 instrument (JASCO, Tokyo, Japan), with a $BaSO_4$ plate as the reference. Powder X-ray diffraction (XRD) was performed using an X-ray diffractometer (LabX XRD-6000, Shimadzu, Kyoto, Japan) with Cu Kα radiation. The thermal diffusivities of the catalysts after reduction pretreatment at 873 K were measured by the laser flash method (LFA 467 HyperFlash, NETZSCH, Selb, Germany), and the specific heat capacity was measured by the differential scanning calorimetry (DSC) method in the range of 273–323 K (DSC-60Plus, Shimadzu corporation, Kyoto, Japan). High-resolution transmission electron microscopy (HR-TEM) images were measured on a JEM-2100F (JEOL, Tokyo, Japan) at the acceleration voltage of 200 kV. Ni K-edge X-ray absorption spectra (XAS) were recorded in a transmission mode at room temperature at the BL9A facility of the Photon Factory, High Energy Accelerator Research Organization (KEK-PF, Tsukuba, Japan) using a Si(111) double crystal monochromator. The reduced samples for XAS measurements were sealed in polyethylene bags immediately after reduction pretreatment (5% H_2/Ar 100 ml min^{-1}, 873 K, 30 min) to minimise oxidation of the Ni species by air.

Photothermal catalytic activity test

Photothermal catalytic activity tests were performed using a fixed-bed flow reactor with irradiation space (2 cm × 2 cm × 1 mm) as described in our previous study.[21] The catalyst powder was pelletised, crushed and sieved into granules (sieve size: 150–300 μm). The catalyst granules were filled in the reactor. The amounts of catalysts differed depending on the density of the catalysts and were summarized in Table S1.† Before the activity test, reduction (5% H_2/Ar, 100 ml min^{-1}, 873 K, 30 min) pretreatment was performed, and then the reactant gas (12.5% CO_2/10% CH_4/5% N_2/Ar, 200 ml min^{-1}) was introduced to the reactor at room temperature. For irradiation of concentrated visible and near-infrared (visible/NIR) light, a 300 W Xe lamp (Cermax PE300BFA, Excelitas Technologies, Massachusetts, USA; light power: 17.3 W) equipped with optical filters (L39, HOYA, Tokyo, Japan, $\lambda > 390$ nm; W-Y435, HOYA, Tokyo, Japan, $\lambda > 435$ nm) and a focusing lens (LGQ30/40P, Eagle Engineering,

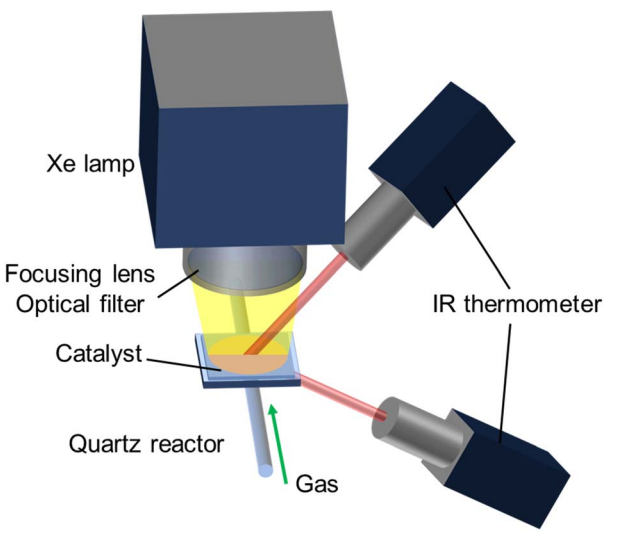

Scheme 1 Setup for catalytic activity evaluation of the PT-DRM reaction.

 This journal is © The Royal Society of Chemistry 2025

Open Access Article. Published on 20 June 2025. Downloaded on 25/11/2025 6:45:27 AM.
This article is licensed under a Creative Commons Attribution-NonCommercial 3.0 Unported Licence.

Tokyo, Japan, irradiation area: Φ 20 mm) was used (Scheme 1). The temperature of the reactor under light irradiation was measured using an infrared (IR) thermometer (TMHX-CGE2400-0150H2.2, JAPANSENSOR, Tokyo, Japan). The outlet gas was analysed by online gas chromatography with a thermal conductivity detector (GC-8A, Shimadzu, Kyoto, Japan) using a Shincarbon ST column.

Thermocatalytic activity test

Thermocatalytic activity tests were performed in the dark using a glass tube (inner diameter: Φ 4 mm). The catalyst granules (50 mg, 25 mg for bare Ni/SiO_2 catalyst) were inserted into the glass tube. After the reduction pretreatment, the reactant gas was introduced to the reactor. The thermocatalytic activities were evaluated at 723 K. The other experimental procedures were identical to those used for the photothermal catalytic activity tests, except that no light irradiation was applied.

Results & discussion

Characterisations of the Ni/SiO_2 and mixed catalysts

From the HR-TEM image of the reduced Ni/SiO_2 catalyst, the mean particle size (d_{TEM}) of Ni NPs was estimated to be 4.6 nm (Fig. 1a and b). The Ni NPs were covered with a thin SiO_2 layer (Fig. S1†), as previously reported.[37] The powder XRD analysis identified peaks attributed to Ni metal ($2\theta = 44.4$, 51.9, and 76.4°) without impurities (Fig. 1c). The crystallite sizes (d_{XRD}) of Ni metal were estimated to be 20 nm from the peak at 51.9° using the Scherrer equation. This difference between d_{TEM} and d_{XRD} would reflect sensitivity of XRD to larger Ni particles.[48] The Ni K-edge XAS measurement also confirmed that Ni species existed as Ni metal in the Ni/SiO_2 catalyst (Fig. 1d). The UV/visible/NIR DR spectra showed absorption in the range of 400–2400 nm in the Ni/SiO_2 catalyst (Fig. 1e), with the visible/NIR absorption attributed to Ni metal NPs, given the absorption of SiO_2.

To prepare mixed catalysts, the Ni/SiO_2 catalyst was physically mixed with ceramics of SiO_2, α-Al_2O_3, AlN, SiC, or TiC in a 1 : 1 weight ratio. The XRD patterns of the mixed catalysts after 5-hour PT-DRM reaction showed only the peaks of the Ni/SiO_2 catalysts and these ceramics without impurities (Fig. 2a). The absence of any shift in Ni peaks indicates that the mixed ceramics were not doped into the Ni metal during the PT-DRM reaction (Fig. S2†). The d_{XRD} values of the mixed catalysts remained ~20 nm (Table S2†), consistent with that of the Ni/SiO_2 catalyst without the ceramic mixing. Ni K-edge XAS measurements also confirmed that Ni species remained mainly as Ni metal among the mixed catalysts (Fig. 2b). The UV/visible/NIR DR spectra showed that all mixed catalysts had a reflectance of ~17% in visible/NIR region (Fig. 2c). Slight variations were observed depending on the ceramics, with a lower reflectance observed in the catalysts mixed with high light-absorbing ceramics (Fig. 2d).

Photothermal activity of the catalysts

The photothermal activity test on the Ni/SiO_2 catalyst showed relatively constant CO and H_2 formation over 5 h, confirming

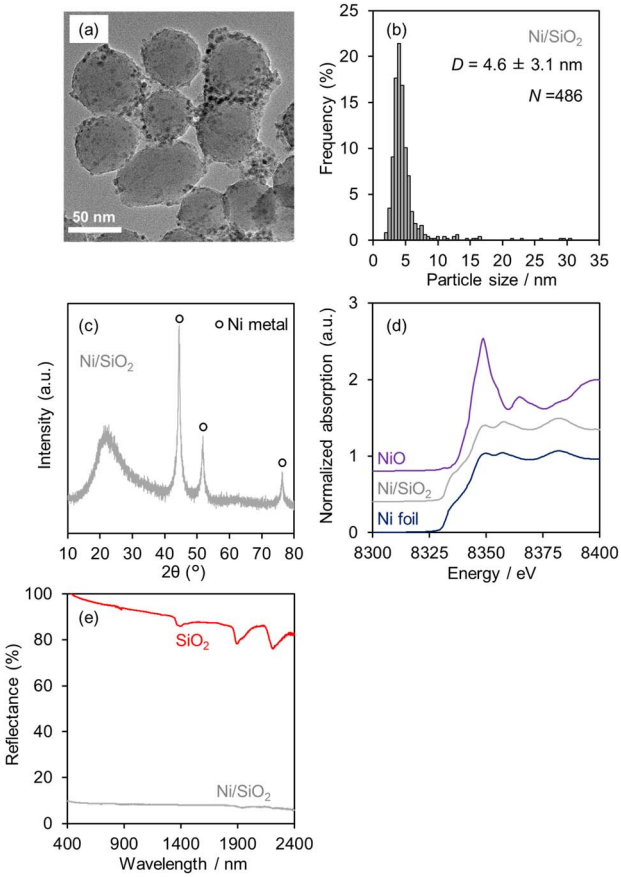

Fig. 1 Characterization results of the Ni/SiO_2 catalyst. (a) HR-TEM image, (b) the particle size distribution of the Ni NPs determined from the HR-TEM images, and (c) XRD pattern of the Ni/SiO_2 catalyst. (d) Ni K-edge XANES spectra of the Ni/SiO_2 catalyst and references. (e) UV-visible-NIR DR spectra of the Ni/SiO_2 catalyst and bare SiO_2. The Ni/SiO_2 catalyst was measured after the reduction pretreatment by 5% H_2/Ar at 873 K.

that the PT-DRM reaction proceeded (Fig. 3a). The slight decline in product formation rates would be due to coke deposition *via* methane decomposition (eqn (2)), as previously reported.[37]

$$CH_4 \rightarrow C + 2H_2 \quad \Delta H^\circ_{298K} = 75.6 \text{ kJ mol}^{-1} \qquad (2)$$

Moreover, the formation rates of CO and H_2 were not equivalent according to the stoichiometry in eqn (1) due to side reactions between H_2 and CO_2, such as the Sabatier reaction (eqn (3)) and the reverse water gas shift reaction (eqn (4)).[30]

$$CO_2 + 4H_2 \rightarrow CH_4 + 2H_2O \quad \Delta H^\circ_{298K} = -165 \text{ kJ mol}^{-1} \qquad (3)$$

$$CO_2 + H_2 \rightarrow CO + H_2O \quad \Delta H^\circ_{298K} = 41.3 \text{ kJ mol}^{-1} \qquad (4)$$

The PT-DRM reaction also proceeded over the mixed catalysts, and their formation rates of CO and H_2 varied among the catalysts (Fig. 3b). While their activities were evaluated with different amounts of catalyst to fix the irradiation area, no direct relationship was observed between catalytic activities and the

Open Access Article. Published on 20 June 2025. Downloaded on 25/11/2025 6:45:27 AM.
This article is licensed under a Creative Commons Attribution-NonCommercial 3.0 Unported Licence.

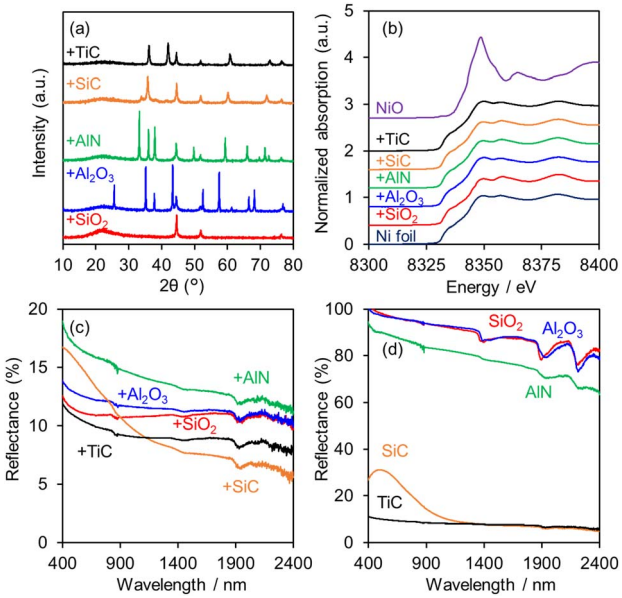

Fig. 2 Characterisation results of the mixed catalysts. (a) XRD patterns of the mixed catalysts after the 5-hour PT-DRM reaction. (b) Ni K-edge XANES spectra of the mixed catalysts after reduction at 873 K and references. UV-vis-NIR DR spectra of (c) the reduced mixed catalysts and (d) the mixed ceramics.

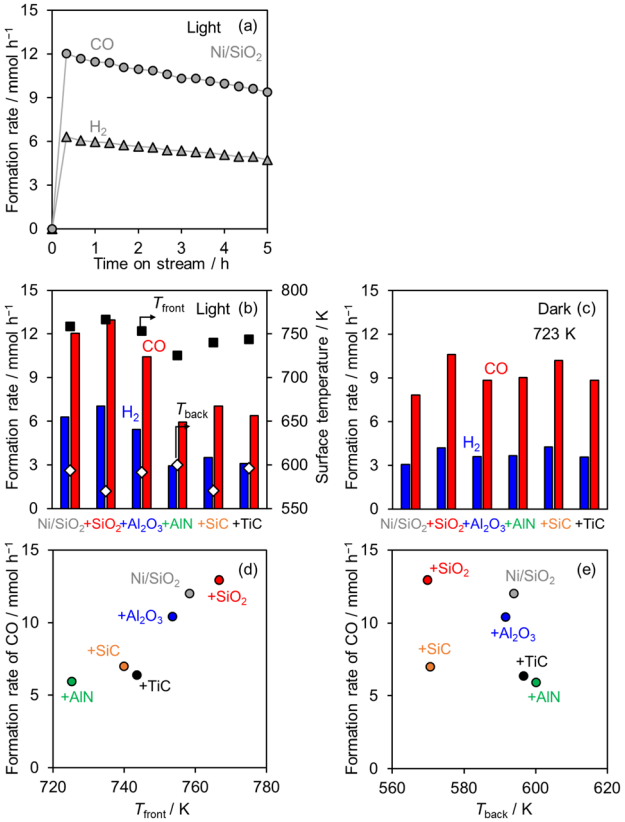

Fig. 3 Catalytic activity of the Ni/SiO_2 catalyst and the mixed catalysts. (a) Time course of formation rate of CO and H_2 over the Ni/SiO_2 catalyst. (b) Photothermal and (c) thermocatalytic activities of the catalysts. Relationship between CO formation rate and surface temperature of the (d) frontside and (e) backside of the reactor measured with the IR thermometer. Feed gas: 12.5% CO_2/10% CH_4/5% N_2/Ar (200 mL min^{-1}) light: λ > 435 nm, 17.3 W, without other additional heating. The formation rate was evaluated at 20 min after light irradiation.

amounts of the Ni/SiO_2 catalyst (Table S1 and Fig. S3†). Moreover, there was little difference in the activities of the thermocatalytic DRM reaction at 723 K in the dark (Fig. 3c), indicating that the catalytic properties of the Ni/SiO_2—such as Ni particle size, reduction state and interaction with SiO_2—remained largely unaffected by the incorporation of the mixed ceramics. Therefore, the differences in the photothermal catalytic activities would be attributed to variations in temperature profiles, primarily caused by differences in heat dissipation under light irradiation.

To further explore this, the temperature of the frontside (T_{front}) and backside (T_{back}) surfaces of the quartz reactor were measured with the IR thermometer. The T_{front} value was much higher than the T_{back} value among all catalysts. The distinctive temperature gradients would be created by the light-driven local heating, a specific feature of photothermal catalysis. Moreover, the T_{front} values varied among the mixed catalysts, positively correlating with the photothermal catalytic activities (Fig. 3d). In contrast, T_{back} values showed no significant correlation with the photothermal catalytic activity (Fig. 3e). These results indicate that catalytic activities are strongly influenced by the highest temperature (*i.e.* T_{front} value) possibly due to the exponential increase in catalytic activity with reaction temperature (Fig. S4†).

Temperature gradient of the mixed catalysts

Next, the factors contributing to the temperature gradients were investigated. The temperature gradients would be derived from the heat dissipation process, particularly thermal conductivity, in the catalyst bed under irradiation. The thermal conductivity measurements revealed that the catalysts with lower thermal conductivities generally exhibited higher T_{front} values and larger temperature gradients, differences between the T_{front} and T_{back} values (Fig. 4a and b). These results suggest that the heat generated on the frontside surface dissipated towards the backside, with the dissipation rate mainly governed by the

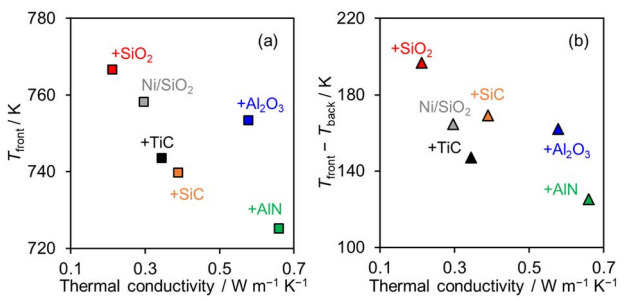

Fig. 4 Effects of thermal conductivity on (a) T_{front} values and (b) temperature difference between the frontside and backside (*i.e.*, $T_{front} - T_{back}$).

This journal is © The Royal Society of Chemistry 2025

Open Access Article. Published on 20 June 2025. Downloaded on 25/11/2025 6:45:27 AM.
This article is licensed under a Creative Commons Attribution-NonCommercial 3.0 Unported Licence.

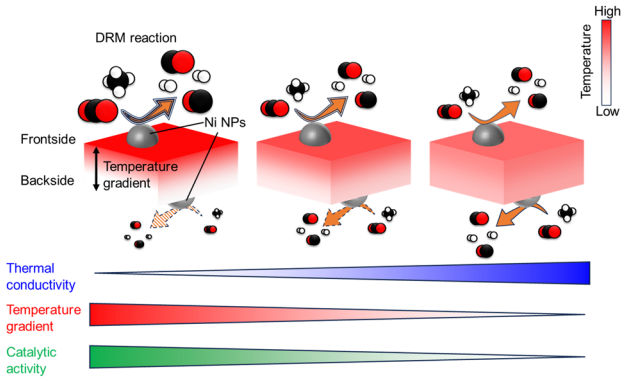

Scheme 2 Effect of thermal conductivity on temperature gradient and catalytic activity.

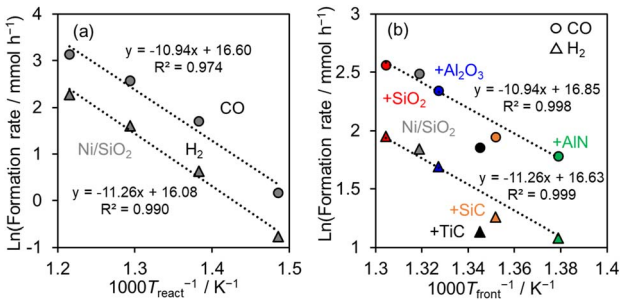

Fig. 5 (a) Arrhenius plot of the Ni/SiO_2 catalyst and (b) relationship between photothermal catalytic activities and T_{front} values of the mixed catalysts.

thermal conductivities of the catalysts. Therefore, catalysts with lower thermal conductivities are more effective for suppressing heat dissipation, resulting in a higher T_{front} value and photothermal catalytic activities as observed in Fig. 3d (Scheme 2).

Effect of the color of the mixed ceramics on the catalytic activity

To further investigate the relationship between temperature and activity for each catalyst, the activation energy (E_a) of the thermal DRM reaction over the Ni/SiO_2 catalyst was calculated to be 90.9 and 93.6 kJ mol^{-1} based on the CO and H_2 formation rates measured in the dark (Fig. 5a, see Fig. S4† for the temperature dependence of activity). Similarly, the natural logarithms of CO and H_2 formation rates were plotted against 1000 T_{front}^{-1} for each catalyst (Fig. 5b). The catalysts mixed with the low light-absorbing ceramics (Ni/SiO_2 +SiO_2, +Al_2O_3, and +AlN) exhibited a strong linear correlation, with a slope identical to that of the Arrhenius plot for the Ni/SiO_2 catalyst. This consistency indicates that the apparent E_a values remain similar among the mixed catalysts.

In contrast, the mixed catalysts with high light-absorbing ceramics (Ni/SiO_2 +SiC and +TiC) deviated from the expected trend, exhibiting lower activity than predicted based on their T_{front} values, despite the minimal differences in the amounts of the Ni/SiO_2 catalyst (Table S1†). The estimated temperatures of Ni NPs, calculated from their CO formation rates and the approximate trend line, were 734 K and 729 K for the Ni/SiO_2 +SiC and +TiC catalysts, respectively. These estimated temperatures were significantly lower than their T_{front} values for highly light-absorbing ceramics (−10.8 and −14.5 K, see Table S3† for the values of all catalysts). This discrepancy would be attributed to significant light absorption by the SiC and TiC ceramics, which are likely to reduce direct light absorption by Ni NPs. These results indicate the effectiveness of the direct light absorption of Ni NPs in enhancing the PT-DRM reaction.

Conclusions

In this study, we investigated the photothermal catalytic activity of ceramics-mixed Ni/SiO_2 catalysts in the photothermal dry reforming of methane reaction, emphasizing the roles of thermal conductivity of catalyst and direct light absorption of nickel nanoparticles. Our findings reveal that lower thermal conductivity of catalysts contributes to increased frontside temperature by minimizing heat dissipation to the backside, resulting in high catalytic activity. Moreover, in this experiment, the irradiated surface temperature was closely correlated with the temperature estimated from the catalytic activity of the catalysts mixed with low light-absorbing ceramics (*i.e.* SiO_2, Al_2O_3, and AlN). In contrast, mixing with high light-absorbing ceramics (*i.e.* SiC and TiC) led to lower catalytic activities relative to the surface temperature, indicating that these ceramics inhibited direct light absorption by Ni NPs.

Overall, this research demonstrates the significance of thermal conductivity and direct light absorption in photothermal catalytic systems. These insights pave the way for the development of more efficient photothermal catalysts for sustainable energy conversion processes, particularly in utilizing renewable solar energy.

Data availability

The data supporting this article have been included as part of the ESI.†

Author contributions

D. T. and A. Y. conceived and directed the project under the supervision of H. Y. D. T. prepared the catalysts, performed the activity tests, and conducted all characterization studies. D. T. wrote the paper with comments from all authors.

Conflicts of interest

There are no conflicts to declare.

Acknowledgements

This work was financially supported by the Scientific Research (B) (21H01975 and 24K01527) from the Japan Society for the Promotion of Science. D. T. thanks financial support from the Japan Science and Technology Agency SPRING (JPMJSP2110).

Open Access Article. Published on 20 June 2025. Downloaded on 25/11/2025 6:45:27 AM. This article is licensed under a Creative Commons Attribution-NonCommercial 3.0 Unported Licence.

XAS was performed at BL9A of the Photon Factory, KEK-PF, Tsukuba, Japan, with the approval of the Photon Factory Program Advisory Committee (Proposal No. 2022G549). The authors thank Mr Kiyomura for the TEM observations, supported by Kyoto University Nano Technology Hub, Kyoto, Japan, under the Nanotechnology Platform Project.

Notes and references

1 M. Asif and T. Muneer, *Renew. Sustain. Energy Rev.*, 2007, **11**, 1388–1413.
2 H. Lund, *Energy*, 2007, **32**, 912–919.
3 A. Soundarya Mary, G. Mahendra, R. Roy, M. K. Ganesha and A. K. Singh, *EES Batter.*, 2025, **1**, 23–72.
4 E. J. Luber, M. H. Mobarok and J. M. Buriak, *ACS Nano*, 2013, **7**, 8136–8146.
5 L. Lahourcade, N. C. Coronel, K. T. Delaney, S. K. Shukla, N. A. Spaldin and H. A. Atwater, *Adv. Mater.*, 2013, **25**, 2562–2566.
6 O. Vazquez-Mena, J. P. Bosco, O. Ergen, H. I. Rasool, A. Fathalizadeh, M. Tosun, M. Crommie, A. Javey, H. A. Atwater and A. Zettl, *Nano Lett.*, 2014, **14**, 4280–4285.
7 B. Huskinson, M. P. Marshak, C. Suh, S. Er, M. R. Gerhardt, C. J. Galvin, X. Chen, A. Aspuru-Guzik, R. G. Gordon and M. J. Aziz, *Nature*, 2014, **505**, 195–198.
8 X. Li, M. Ibrahim Dar, C. Yi, J. Luo, M. Tschumi, S. M. Zakeeruddin, M. K. Nazeeruddin, H. Han and M. Grätzel, *Nat. Chem.*, 2015, **7**, 703–711.
9 L. Zhou, Y. Tan, J. Wang, W. Xu, Y. Yuan, W. Cai, S. Zhu and J. Zhu, *Nat. Photonics*, 2016, **10**, 393–398.
10 M. Ghoussoub, M. Xia, P. N. Duchesne, D. Segal and G. Ozin, *Energy Environ. Sci.*, 2019, **12**, 1122–1142.
11 Y. Wang, H.-M. Meng, G. Song, Z. Li and X.-B. Zhang, *ACS Appl. Polym. Mater.*, 2020, **2**, 4258–4272.
12 Y. Zou, Y. Zhang, Q. Yu and H. Chen, *Biomater. Sci.*, 2021, **9**, 10–22.
13 A. Fujishima and K. Honda, *Nature*, 1972, **238**, 37–38.
14 S. Malato, J. Blanco, C. Richter and M. I. Maldonado, *Appl. Catal. B Environ.*, 2000, **25**, 31–38.
15 S. Shoji, X. Peng, A. Yamaguchi, R. Watanabe, C. Fukuhara, Y. Cho, T. Yamamoto, S. Matsumura, M.-W. Yu, S. Ishii, T. Fujita, H. Abe and M. Miyauchi, *Nat. Catal.*, 2020, **3**, 148–153.
16 H. Nishiyama, T. Yamada, M. Nakabayashi, Y. Maehara, M. Yamaguchi, Y. Kuromiya, Y. Nagatsuma, H. Tokudome, S. Akiyama, T. Watanabe, R. Narushima, S. Okunaka, N. Shibata, T. Takata, T. Hisatomi and K. Domen, *Nature*, 2021, **598**, 304–307.
17 W. Zhou, W. Li, J.-Q. Wang, Y. Qu, Y. Yang, Y. Xie, K. Zhang, L. Wang, H. Fu and D. Zhao, *J. Am. Chem. Soc.*, 2014, **136**, 9280–9283.
18 K. Wang, Q. Li, B. Liu, B. Cheng, W. Ho and J. Yu, *Appl. Catal. B Environ.*, 2015, **176–177**, 44–52.
19 S. Wang, B. Zhu, M. Liu, L. Zhang, J. Yu and M. Zhou, *Appl. Catal. B Environ.*, 2019, **243**, 19–26.
20 T. Takata, J. Jiang, Y. Sakata, M. Nakabayashi, N. Shibata, V. Nandal, K. Seki, T. Hisatomi and K. Domen, *Nature*, 2020, **581**, 411–414.
21 D. Takami, A. Yamamoto and H. Yoshida, *Catal. Sci. Technol.*, 2020, **10**, 5811–5814.
22 M. Ghoussoub, M. Xia, P. N. Duchesne, D. Segal and G. Ozin, *Energy Environ. Sci.*, 2019, **12**, 1122–1142.
23 Y. Ren, S. Lan, Y.-H. Zhu, R. Peng, H. He, Y. Si, K. Huang and N. Li, *ChemSusChem*, 2025, e202402485.
24 Z. Xiao, L. Zhang, X. Tan, K. Sun, J. Li, L. Pan, J.-J. Zou, G. Li and D. Wang, *Adv. Funct. Mater.*, 2025, 2500339.
25 M. Pagliaro, R. Ciriminna, H. Kimura, M. Rossi and C. Della Pina, *Angew. Chem., Int. Ed.*, 2007, **46**, 4434–4440.
26 H. Liu, T. D. Dao, L. Liu, X. Meng, T. Nagao and J. Ye, *Appl. Catal. B Environ.*, 2017, **209**, 183–189.
27 H. Liu, X. Meng, T. D. Dao, L. Liu, P. Li, G. Zhao, T. Nagao, L. Yang and J. Ye, *J. Mater. Chem. A*, 2017, **5**, 10567–10573.
28 H. Huang, M. Mao, Q. Zhang, Y. Li, J. Bai, Y. Yang, M. Zeng and X. Zhao, *Adv. Energy Mater.*, 2018, **8**, 1–11.
29 Q. Zhang, M. Mao, Y. Li, Y. Yang, H. Huang, Z. Jiang, Q. Hu, S. Wu and X. Zhao, *Appl. Catal. B Environ.*, 2018, **239**, 555–564.
30 D. Takami, Y. Ito, S. Kawaharasaki, A. Yamamoto and H. Yoshida, *Sustain. Energy Fuels*, 2019, **3**, 2968–2971.
31 K. Takeda, A. Yamaguchi, Y. Cho, O. Anjaneyulu, T. Fujita, H. Abe and M. Miyauchi, *Glob. Challenges*, 2020, **4**, 1900067.
32 X. Liu, H. Shi, X. Meng, C. Sun, K. Zhang, L. Gao, Y. Ma, Z. Mu, Y. Ling, B. Cheng, Y. Li, Y. Xuan and Y. Ding, *Sol. RRL*, 2021, **5**, 2100185.
33 K. Han, Y. Wang, S. Wang, Q. Liu, Z. Deng and F. Wang, *Chem. Eng. J.*, 2021, **421**, 129989.
34 T. Xie, Z. Y. Zhang, H. Y. Zheng, K. D. Xu, Z. Hu and Y. Lei, *Chem. Eng. J.*, 2022, **429**, 132507.
35 K. Lorber, J. Zavašnik, J. Sancho-Parramon, M. Bubaš, M. Mazaj and P. Djinović, *Appl. Catal. B Environ.*, 2022, **301**, 120745.
36 X. Liu, Z. Mu, C. Sun, H. Shi, X. Meng, P. Li, Y. Ling, B. Cheng, Y. Xuan and Y. Ding, *Fuel*, 2022, **310**, 122441.
37 D. Takami, J. Tsubakimoto, W. Sarwana, A. Yamamoto and H. Yoshida, *ACS Appl. Energy Mater.*, 2023, **6**, 7627–7635.
38 J. Cheng, X. Liu, T. Li, D. Li, Z. Jiang, D. Xu, B. Patel and Y. Guo, *Int. J. Hydrogen Energy*, 2024, **53**, 1433–1444.
39 A. Yamamoto, M. Sugitani, D. Takami, K. Kato, T. Shishido and H. Yoshida, *J. Japan Pet. Inst.*, 2024, **67**, 217–223.
40 Z. Cai, Y. Cai, Z. Wang, S. Liu, X. Liang, H. Ren, Y. Cao, Z. Su, F. Shen, S. Yang, G. Sun, X. Yang, X. Zhang, M. Hu, X. Liu and K. Zhou, *Chem. Eng. J.*, 2024, **498**, 155554.
41 H. A. El-Naggar, D. Takami, H. Asanuma, T. Hirata, H. Yoshida and A. Yamamoto, *ChemCatChem*, 2024, e202401396.
42 L. Meng, Y. Jia and S. Wu, *Chem. Commun.*, 2025, **61**, 2301–2304.
43 Y. Zhang, Q. Zhang, Y. Luo and S. Wu, *Mol. Catal.*, 2025, **573**, 114844.
44 X. Tian, Y. Shi, J. Zhang and F. Wang, *Green Energy Environ.*, 2025, DOI: **10.1016/j.gee.2025.02.008**.

 This journal is © The Royal Society of Chemistry 2025

Open Access Article. Published on 20 June 2025. Downloaded on 25/11/2025 6:45:27 AM.
This article is licensed under a Creative Commons Attribution-NonCommercial 3.0 Unported Licence.

45 H. A. El-Naggar, H. Yoshida and A. Yamamoto, *Sustain. Energy Fuels*, 2025, **9**, 1596–1604.
46 H. A. El-Naggar, H. Asanuma, H. Yoshida and A. Yamamoto, *Sol. RRL*, 2025, **9**, 2500021.
47 S. Arora and R. Prasad, *RSC Adv.*, 2016, **6**, 108668–108688.
48 W. Sarwana, D. Takami, A. Yamamoto and H. Yoshida, *Catal. Sci. Technol.*, 2023, **13**, 1755–1762.